Hindawi
Mathematical Problems in Engineering
Volume 2022, Article ID 5419671, 10 pages
https://doi.org/10.1155/2022/5419671

Research Article

A CFD Study on the Design Optimization of Airborne Infection Isolation Room

Thanh-Long Le,[1,2,3] **Tan Tien Nguyen**,[1,2,3] **and Trung Tin Kieu**[1,3]

[1]*Faculty of Mechanical Engineering, Ho Chi Minh City University of Technology (HCMUT), 268 Ly Thuong Kiet Street, District 10, Ho Chi Minh, Vietnam*
[2]*National Key Laboratory of Digital Control and System Engineering (DCSELab), HCMUT, 268 Ly Thuong Kiet Street, District 10, Ho Chi Minh, Vietnam*
[3]*Vietnam National University Ho Chi Minh City, Linh Trung Ward, Thu Duc City, Ho Chi Minh, Vietnam*

Correspondence should be addressed to Thanh-Long Le; ltlong@hcmut.edu.vn

Received 12 April 2022; Revised 15 August 2022; Accepted 18 September 2022; Published 3 October 2022

Academic Editor: Adnan Maqsood

Airborne infection isolation (AII) rooms are used to accommodate patients with highly infectious diseases and keep the released pathogens to limit the risk of cross-infection. This paper proposes a concept for an AII room made from two shipping containers to handle the scarcity of hospital beds when the COVID-19 disease spreads over the world. The proposed system consists of the main isolation room, anteroom, and toilet as well as other functional areas. In addition, the main isolation room was modeled with important components such as a supply air vent, exhaust air, a patient, and a bed. The computational fluid dynamics (CFD) approach based on the finite volume method (FVM) is used to solve the three-dimensional governing equations. The CO_2 concentration was used to determine the infectious contaminant concentration of the air in the room. Therefore, the infectious control could be evaluated by the air change per hour (ACH). The numerical results show that the room temperature is maintained at 24°C, which is appropriate for people in the room. The laminar airflow extends downward to the floor after leaving the supply air vent on the ceiling, creating circulating patterns throughout the room. When evaluating the effectiveness of ventilation systems to remove airborne contaminants based on different ACH numbers, the CO_2 concentration in the room was reduced to 581 ppm, 477 ppm, and 438 ppm in the cases of 12 ACH, 24 ACH, and 48 ACH, respectively. As a result, the greater the number of air change per hour, the greater the performance for contaminant removal. It served as the foundation for assessing and optimizing the ventilation system of the portable negative pressure room.

1. Introduction

In early 2020s, we witnessed an alarming outbreak of COVID-19, a severe respiratory disease caused by the novel SARS-CoV-2, across over 180 countries in the world. The study has shown that the transmission of SARS-CoV-2 could be generated through respiratory droplets and small aerosols [1]. This has led to extensive research on infections and infection control in both outdoor and indoor environments [2–6]. A logical solution to minimizing disease transmission was the isolation of the infected patient. Ventilation in hospitals and buildings plays an important role in controlling airborne infections [7]. In hospitals, patients with airborne infectious diseases are typically placed in airborne infection isolation (AII) rooms or commonly called negative pressure rooms. When compared to the corridor and other adjacent spaces, these rooms are under negative pressure. The function of the negative pressure is to direct airflow towards the isolation room, preventing the spread of airborne infections to the surrounding regions. Containment of airborne contaminants minimizes the possibility of cross-infection outside of the isolation room.

Computational fluid dynamics (CFD) simulation is a valuable technology for the understanding of hydroaerodynamics in many areas such as evaluating fluid

motion and hydrodynamic characteristics (pressure and velocity) in a microchannel, sterilization chamber, or laminar airflow unit in operating rooms [8–13]. Beaussire et al. [14] performed CFD simulations based on the lattice Boltzmann method (LBM) to analyze the airflow and particles spreading from a patient's cough, and summer and winter weather effects are also considered in the study. In the isolation room study, the CFD method is used to study the air quality, comfort level, the performance of the HVAC system, the air streamline, pressurization, contaminants transportation, etc. [15]. The airflow characteristics in the AII room play an important role in increasing or reducing the spreading of infection in the whole room. Therefore, it is well known that the design of isolation rooms is closely related to indoor airflow. A variety of research studies involving negative pressure isolation rooms have been carried out using CFD numerical analysis. A study by Suvanjan Bhattacharyya et al. [16] indicated the use of CFD simulation in minimizing the spread of the COVID-19 virus in a hospital isolation room. Their model combines conditioned airflow from an air conditioner mixed with an aerosol sanitizer to kill or minimize viruses in the isolation room. They applied CFD to analyze temperature, turbulent kinetic energy, and aerodynamics, which impact aerosol sanitizer delivery systems and allow them to reach every corner of the room. Thatiparti et al. [17] found that the flow path between the patient contaminant source and the outlet vent is the most important factor for infectious aerosol control. The location of the outlet vent is closer to the patient, and the movement of clean air from the clean space in the room to the contaminated space is the most effective method of controlling infection in a negative pressure room. It should also be emphasized that removing infectious aerosols from the room is difficult even though the alternative mock AIIR ventilation protects healthcare workers from risk exposure very well. An experiment and simulation have been conducted by King et al. [18] to evaluate the spatial distribution of aerosols in a hospital negative pressure room. While using the CFD technique to investigate indoor air, the turbulence model should be carefully considered. Using the RSM turbulent model to analyze bioaerosol deposition has helped to solve the anisotropic nature of the flow better than the frequently used $k-\varepsilon$ turbulent model, increasing the accuracy of the numerical results compared to the experimental data. Sheller et al. [19] had modified existing HVAC systems in the ward of a skilled nursing facility to create a temporary and emergency negative pressure environment. These modifications were not resource-intensive and time-consuming when the number of patients surged during a pandemic. Numerical and experimental results are consistent and meet the CDC guidelines. Thus, the community will benefit when medical facilities for isolation and treatment of infectious diseases are expanded. Shih et al. [20] presented numerical equations and numerical methods to investigate the effects of a moving person and sliding door movement on the air distribution in a negative pressure isolation room. According to the results, contaminants removal was influenced by specified pressure differentials during room closure regardless of the speed at which the person in the room moves. Mahajan et al. [21] used the CFD technique to study steady-state conditions of the negative pressure room with one patient and one stationary human using parameters such as temperature, velocity, pressure, and CO_2 concentration. Jacob et al. [22] reported a study on the influence of the air supply, exhaust vent, and patient's bed position. They found that the location of the immune-suppressed patient's bed should be near the supply air sidewall; meanwhile, the infectious patient's bed should be placed near the exhaust air vent. A transient CFD simulation of a negative pressurized isolation room in Taiwan has been carried out by Wang et al. [23] to improve the room ventilation performance. The results showed that it can be improved by relocating the exhaust air vent closer to the patient's head. However, the hospital's original negative pressure room design still can be improved by using an air-jet curtain with a speed of 0.5 m/s to minimize the distribution of contaminated aerosols and therefore increases medical staff protection. Cho [24] found that the locations of supply air and the exhaust vent are the factors that have the greatest influence on pollutants dispersion in negative pressure rooms. The numerical results have been validated by experimental measurements, demonstrating that the predictions of pollutant concentrations and airflow characteristics are accurate and reliable. Obeidat et al. [25] explored how coronavirus dispersal is affected by suction pressure and airflow velocity in hospital emergency departments by evaluating turbulent kinetic energy and flow dynamics. Numerical simulation and field measurement of a newly constructed pediatric intensive care unit (PICU) isolation room was carried out by Wang et al. [26]. The results help in evaluating ventilation options and selecting the optimal solution for the medical staff and patients in the room. The effects of opening and closing the door of a negative pressure isolation room on the dispersion of infectious particulates have been investigated by Tung et al. [27].

Although there have been many studies on negative pressure rooms, most of them focus on improving the design of existing HVAC systems, analyzing the airflow patterns of permanently built rooms in hospitals. In Vietnam and many other countries around the world, when the number of infected patients increased rapidly, hospitals were overwhelmed leading to delays in receiving hospitalized patients and many unfortunate events occurred. Therefore, it is necessary to have plans to build AII rooms quickly from available materials on the market to be deployed and used in public places such as squares, schools, stadiums, and temporary hospitals, to increase the health system's pandemic response capacity. This paper provides a standard airborne infection isolation room design including a main room, anteroom, and toilets with two 20-foot containers. Moreover, the model was analyzed by the CFD method to evaluate the parameters of velocity, pressure, streamline, carbon dioxide (CO_2) concentration, and ability to transport pathogens

from the room to the filter of the internal airflow under different operating conditions such as 12, 24, and 48 ACH, respectively.

2. Design

Figure 1 shows the three-dimension model of a portable airborne infection isolation room with two 20-foot shipping containers. The projections and external dimensions of the model are shown in Figure 2. The system is 6060 mm in length and 6142 mm in width with a total height of 4575 mm. The system is neatly and squarely constructed for easy travel, deployment, and operation. The container's bottom is equipped with additional support legs that raise the floor higher than the ground, balancing the room against various uneven terrains and preventing rain, mud, soil, and rocks from the ground. The top has a roof to cover the whole system, particularly the equipment installed above the container's roof.

An air handling unit located on the roof of the container is used to distribute the air into the isolation room and the anteroom, as shown in Figure 3. Fresh air will be delivered to the rooms through equal size square air diffusers mounted on the container ceiling. Besides that, the exhaust air will be removed through three equal size wall-mounted exhaust vents right beside the patient's bed. Negative pressure in the room is automatically controlled by a system consisting of pressure sensors and a supply/exhaust airflow rate controllers. Figure 4 displays the layout inside the shipping containers AII room. The system operates as a standard negative pressure room with an anteroom, a toilet, and the main room. The rooms are divided by completely automated sliding doors. The room is designed to be closed to keep humans and the surrounding space safe. The anteroom is located at the end of the main entrance before the main room's door. The space and structure in the main room can satisfy the demands of adding a bedside table, chairs, small refrigerator, television, or specialized equipment and machinery, allowing it to become a temporary negative pressure intensive care unit when critically ill COVID-19 patients hospitalized increase. An inverter controls the exhaust gas flow velocity according to the pressurization parameters to maintain negative pressure in the isolation room.

3. Methodology

3.1. Physical Model. The numerical study concentrated on analyzing the airflow patterns and contaminant removal in the main isolation room; therefore, many solid parts that do not affect the calculation process were ignored to simplify the computational simulation. Figure 5 illustrates the 3D model of the main room including a patient and a bed. The dimensions of the room were 5.896 meters (length), 2.392 meters (width), and additional flooring with dimensions of 1.216×1.652 meters. The room has a total floor area of 16.1 square meters and a ceiling height of 2.329 meters; therefore, its volume is approximately 37.5 cubic meters. The ventilation system operates with a full fresh air supply. The supply air is delivered into the room through a 200 mm square

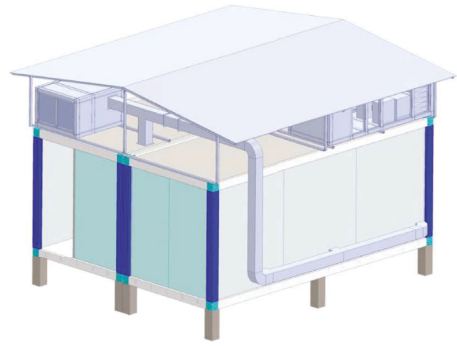

Figure 1: Design of AII room with containers.

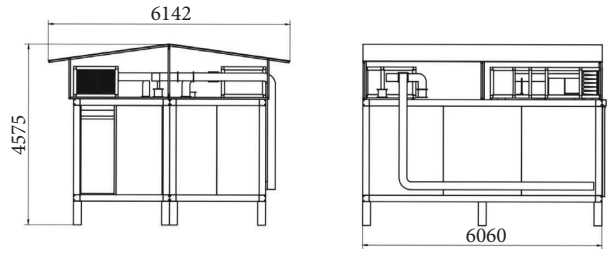

Figure 2: Dimensions of AII room with containers.

diffuser positioned towards the middle of the room on the ceiling. The polluted air will be removed through three 200 mm square wall-mounted exhaust vents right beside the patient's bed. These grilles are 150 mm above the ground and approximately 1700 to 2000 mm apart. The study had a patient with a height of 1700 mm lying on a bed at the height of 600 mm from the floor to the right of the room entrance. The patient's mouth dimensions for width and length are 70 mm and 40 mm, respectively.

The airborne infection isolation room design conditions have to follow the standards of the Vietnamese Ministry of Health, as well as those of many other nations across the world. The air change rate per hour in a negative pressure room should be at least 12 ACH and maintain a pressure differential of 5 to 10 Pa below atmospheric pressure. Moreover, the temperature should be kept between 21 and 26°C. The air change rate per hour inside the room could be found by the rate of supply airflow required for appropriate ventilation of a room, determined by the room's dimension. In this study, the air change rate per hour is calculated by

$$ACPH = \frac{Q_{\text{in}}}{V_{\text{room}}}, \tag{1}$$

where ACPH is the number of air change rates per hour; Q_{in} is the volumetric flow rate of air in cubic meters per hour (m^3/h); and V_{room} is the room volume in cubic meters.

Monitoring carbon dioxide (CO_2) can ensure ventilation performance, air exchange, and air quality in an indoor environment, especially in hospitals [28]. According to Laurent et al. [29], indoor air CO_2 concentrations can also be a measure of the risk of transmission of respiratory pathogens. Ha et al. [30] also used the measurement of carbon dioxide concentration to assess ventilation in the acute care

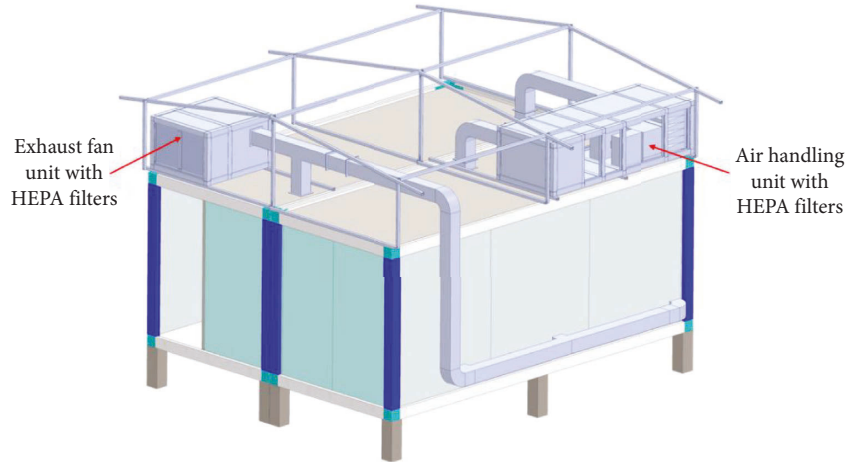

Figure 3: HVAC system of the negative pressure room.

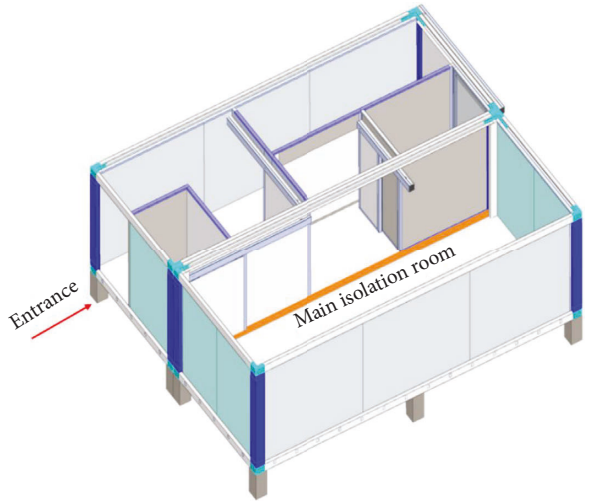

Figure 4: Layout of space inside the room.

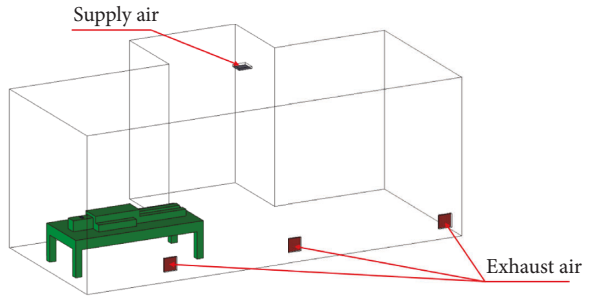

Figure 5: Model of the main isolation room for computational analysis.

hospital. Therefore, in this study, CO_2 concentrations were considered as a contamination source to evaluate the ventilation system's capability in the air renewing process, assuring the safety of the patient and medical staff. Elevated CO_2 concentrations due to patient exhalation were seen as an increase in the concentration of contaminants in the room. According to Kim [31], the CO_2 concentrations in the outdoor air are approximately 400 parts per million (ppm). CO_2 concentrations in human exhalation were about 38000 parts per million. The initial condition of CO_2 concentration in the room was estimated to be 1000 ppm.

The gases from the supply air vent and patient's mouth were composed of air and CO_2 only, and their temperature was assumed to be 22°C and 37°C, respectively. The flow rate of the supply air vent in the case of 24 ACH was 0.25 m^3/s. Boundary conditions of velocity inlets were used to calculate the fluxes of momentum, energy, and species. The pressure at the three exhaust vents was set at −10 Pa and is referred to as ambient pressure. The boundary conditions of the outlet static pressure of the fluid at the outlet plane extrapolate all other conditions from the domain's interior. Heat flux generated from the patient's body was 34.87 W/m^2, and the convection heat transfer coefficient of the walls was 14.7 $W/m^2{\cdot}K$. For the sake of simplicity, no other heat source air infiltration via the doors and windows has been considered, and so it is thought logical to assume the room as one with no doors or windows. The boundary conditions were summarized in Table 1.

3.2. Numerical Methods. In this study, ANSYS Fluent was used to simulate airflow flow physics based on the finite volume method. The equations that determine flow physics include continuity, momentum, and energy, and they follow the concept of conservation as

$$\frac{\partial \rho}{\partial t} + \nabla(\rho V) = 0,$$

$$\frac{\partial}{\partial t}(\rho u_i) + \frac{\partial}{\partial x_i}(\rho u_i u_j) = -\frac{\partial p}{\partial x_i} + \frac{\partial}{\partial x_j}\left(\mu \frac{\partial u_i}{\partial x_j} - \rho \overline{u_i' u_j'}\right),$$

$$\frac{\partial}{\partial t}(\rho E) + \nabla \cdot [\vec{v}(\rho E + p)] = \nabla \cdot \left(k_{\text{eff}} \nabla T - \sum_j h_j \vec{J}_j + \overline{\overline{\tau}}_{\text{eff}} \cdot \vec{v}\right) + S_h. \quad (2)$$

Table 1: Boundary conditions for numerical analysis.

Parameters	Supply air	Exhaust air	Air from patient
Velocity, m/s	6.25	—	0.17
Pressure, Pa	—	−10	—
CO_2 concentration, ppm	400	—	38000
Temperature, ˚C	22	28	37

There is a link between pressure and velocity in the aforementioned equations. The transient, three-dimensional, compressible Navier–Stokes equations, which include gravity, were solved with pressure-velocity coupling using the semi-implicit pressure-linked equations (SIMPLE) algorithm. Over each control volume, the SIMPLE algorithm iteratively solved for the above governing equations. The energy equation was also used to account for temperature variations. The transport equations were discretized using a second-order upwind scheme, with temporal terms discretized using a second-order implicit scheme. The turbulence model was realizable k–ε. This model is widely used for calculating turbulent flow by solving two transport equations: the kinetic energy equation (k) and turbulent dissipation equation (ε).

The kinetic energy equation (k) is written as

$$\frac{\partial}{\partial t}(\rho k) + \frac{\partial}{\partial x_j}\left(\rho k u_j\right) = \frac{\partial}{\partial x_j}\left[\left(\mu + \frac{\mu_t}{\sigma_k}\right)\frac{\partial_k}{\partial x_j}\right] + P_k + P_b - \rho - Y_M + S_k. \tag{3}$$

The turbulent dissipation equation (ε) is described as

$$\frac{\partial}{\partial t}(\rho\varepsilon) + \frac{\partial}{\partial x_j}\left(\rho\varepsilon_j\right) = \frac{\partial}{\partial x_j}\left[\left(\mu + \frac{\mu_t}{\sigma_\varepsilon}\right)\frac{\partial\varepsilon}{\partial x_j}\right] + \rho C_1 S_\varepsilon - \rho C_2 \frac{\varepsilon^2}{k + \sqrt{\nu\varepsilon}} + C_{1\varepsilon}\frac{\varepsilon}{k}C_{3\varepsilon}P_b + S_\varepsilon, \tag{4}$$

where $C_1 = \max[0.43;\ (\eta/(\eta+5))]$; $\eta = S(k/\varepsilon)$; $S = \sqrt{2S_{ij}S_{ji}}$; u_j is the velocity component in the corresponding direction; μ_t is the eddy viscosity; $\mu_t = \rho C_\mu (k^2/\varepsilon)$; $C_\mu = 0.09$; $\sigma_k = 1$; $\sigma_\varepsilon = 1.3$; and $C_{1\varepsilon} = 1.44$.

The aerodynamic characteristics of the main isolation room and detailed views of important components are numerically investigated by CFD simulations in the present study. For a challenging problem, the airflow physics variables change significantly inside the main isolation room and around important components' surfaces. A dense mesh must be located in the main isolation room and detailed views of important components surface during the actuation process guarantee the exact solution. Therefore, the arbitrary Lagrangian–Eulerian (ALE) method is used to handle this problem. On the other hand, the 3-D governing equations with the relevant boundary conditions are solved by using the finite volume method (FVM) with a second-order Lagrange triangular element. The dependency of the number of elements on the numerical results is determined to guarantee the exact solution. The poor quality of mesh elements can lead to collapse and inverts the mesh, and elements could be wrapped inside-out or have zero volume. In this main isolation room model, the mesh structure generated by a polyhedral shapes meshing technique is proposed. The refined mesh was generated at important areas such as the inlet, outlet, and patient's mouth which was carried out for ensuring the accuracy of the numerical results.

The computational domain was divided into small cells that have polyhedral shapes. The meshing module of ANSYS Fluent was used to generate meshes. The refined mesh was generated at important areas such as the inlet, outlet, and patient's mouth. There were 501685 nodes and 188894 cells used in total. Transient numerical simulations were used to calculate aerodynamic parameters and concentration levels and were recorded for 900 seconds. Figure 6 shows the meshing of the main isolation room and detailed views of important components.

4. Results and Discussion

Figure 7 depicts the temperature distribution as a result of numerical simulation at 900 s. The exhaled air mouth was the higher temperature region above the patient's head. The temperature of exhaled air was adjusted to 310.15 K. The cold air from the supply vent spread throughout the room. According to the figure, the temperature distribution in the room at the time 900 s is quite uniform, with an average value of almost 297.15 K. This is the appropriate air temperature for the persons in the room.

Figure 8 illustrates the flow visualization results for different time instants. The laminar airflow left the supply air vent and extended downward to the room's floor before spreading out thoroughly across the main isolation room. Most of the air from the supply air will exit the outlet on the wall in the first few seconds, with only a few creating small vortices (Figure 8(a)). When the system is stabilized (Figure 8(b)–8(e)), the airflow in the room creates a recirculating pattern in multiple directions before reaching the wall-mounted exhaust. Some of the air that has just exited the supply vent flows over the patient's bed before being remixed with the fresh air.The patient's breathing of contaminated air could go along this flow to the outlet. The displayed color shows that the air velocity changes in a decreasing direction. The air from the inlet vent flows at the fastest speed, then slows to become the slowest while in the recirculating pattern, and then accelerates in the room floor area before reaching the outlet. Figure 9 provides a more detailed view of the velocities at several locations in the room. Point P2 near the flow under the inlet reaches the highest velocity at 1.2 m/s. While the remaining points have the same flow velocity at about 0.26 m/s, with no anomalies.

Figure 10 presents CO_2 concentration distribution within the room at different time instants. A greater concentration of airborne contaminants occurred above the patient's body. As time increases, the concentration of CO_2

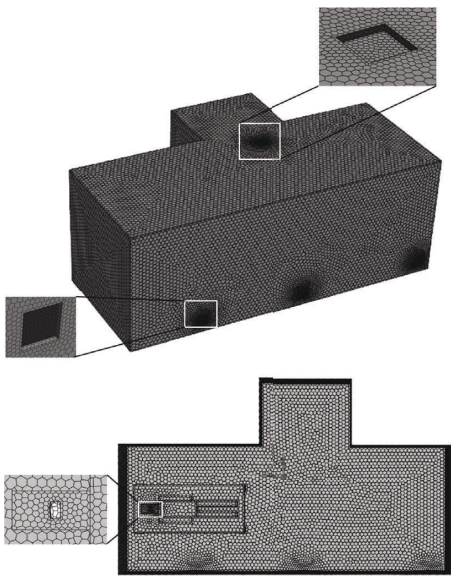

Figure 6: Meshing of the isolation room and detailed views of important components.

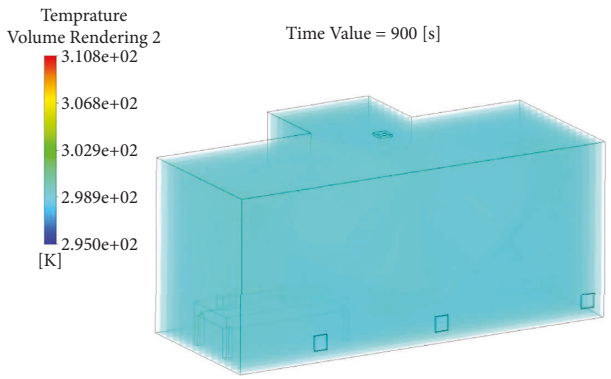

Figure 7: Temperature inside the isolation room at $t = 900$ s.

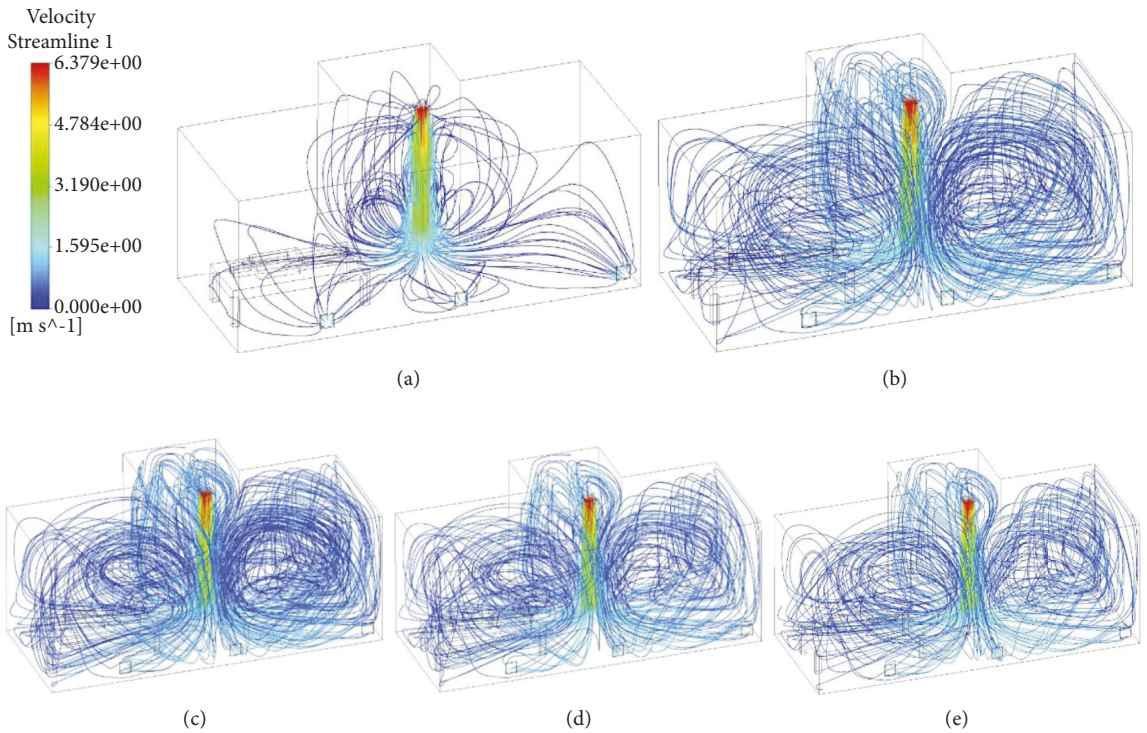

Figure 8: Streamline velocity of supply air in case 24 ACH when $t = 1$ s (a), $t = 225$ s (b), $t = 450$ s (c), $t = 675$ s (d), and $t = 900$ s (e).

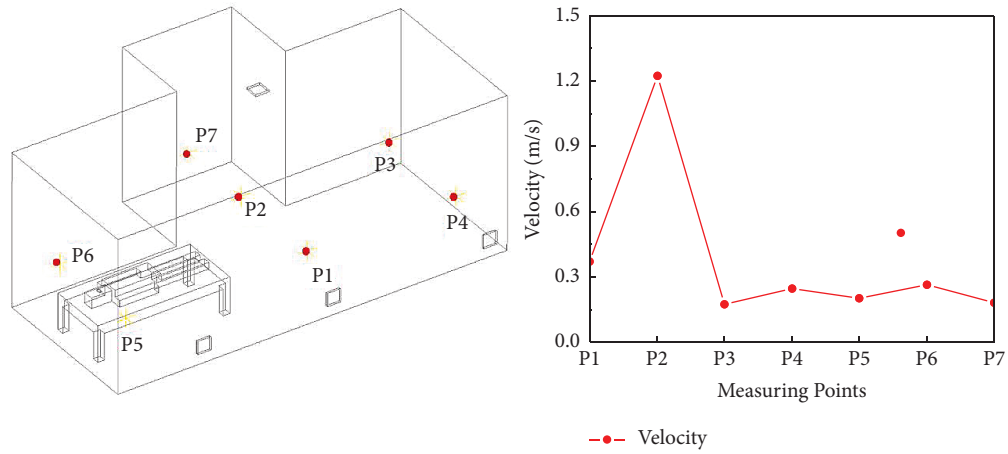

Figure 9: Velocity distribution at various locations inside the room in the case 24 ACH.

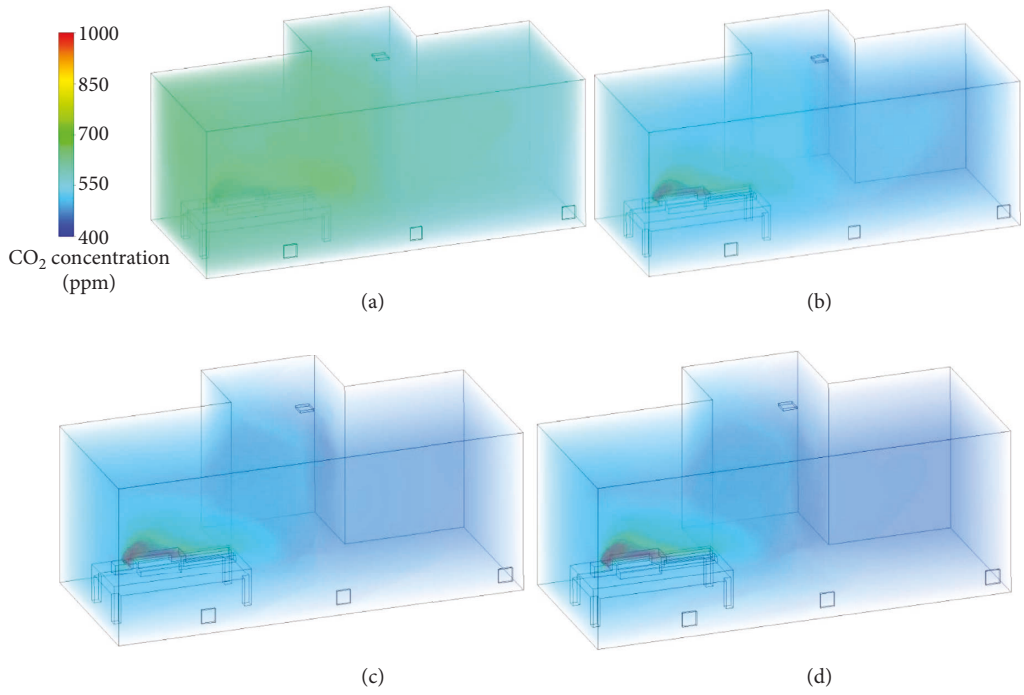

Figure 10: CO_2 concentration distribution pattern in the case 24 ACH when $t = 225$ s (a), $t = 450$ s (b), $t = 675$ s (c), and $t = 900$ s (d).

in the room decreases. When the HVAC system has come into stable operation, the air area that has a high contaminant concentration only occupies a small space in the patient area. The surrounding area has concentrations close to normal. This is important because it represents the ability of the HVAC system to clean the air in the room, representing the exposure of airborne contaminants to medical staff. From the graph shown in Figure 11, in the case of 24 ACH, over 900 s duration, the CO_2 concentration reduced to 477 ppm. This level is slightly higher than 400 ppm of outdoor air. The time interval from 0 to 600 s represents the most significant decrease in the CO_2 concentration in the isolation room. Following then, it changed only very little and nearly attained stability.

Figure 12 is a graph showing the change of the minimum pressure in the room. In the first seconds when the system starts operating, fresh air is pumped into the room through the supply vent, disturbing the pressure in the room leading to a sharp change in the curve from −-7.4 Pa to nearly −10 Pa and then stabilizes over time to an approximate value of −9.5 Pa. When this parameter is compared to the 12 ACH and 48 ACH cases, as shown in Figure 13, the pressure curve trend is the same in all three scenarios. There is a dramatic reduction in pressure in the early seconds, followed by stability over time. The pressure value grows in proportion to the number of air change per hour. 12 ACH case has a minimum pressure of −9.8 Pa, whereas 48 ACH case has a minimum pressure of −7.8 Pa.

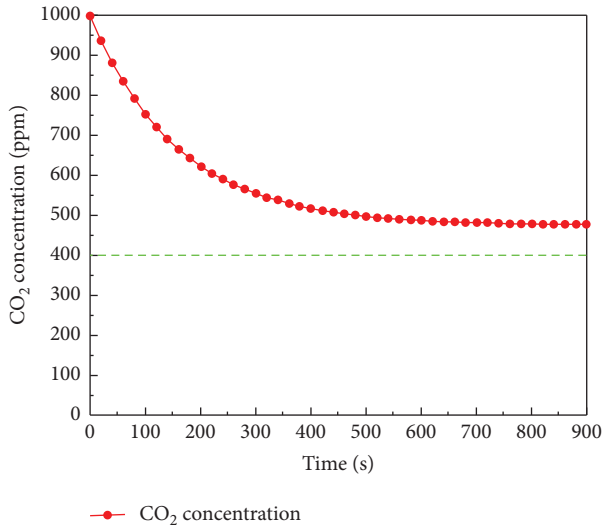

Figure 11: CO_2 concentration in 900 s in the case 24 ACH.

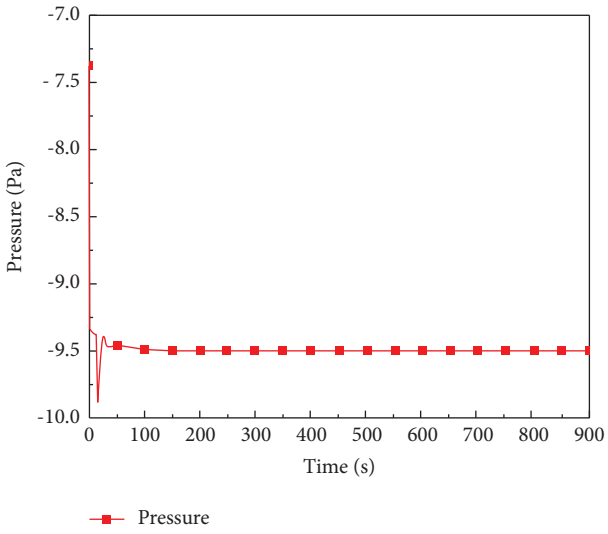

Figure 12: Pressure in 900 s in the case 24 ACH.

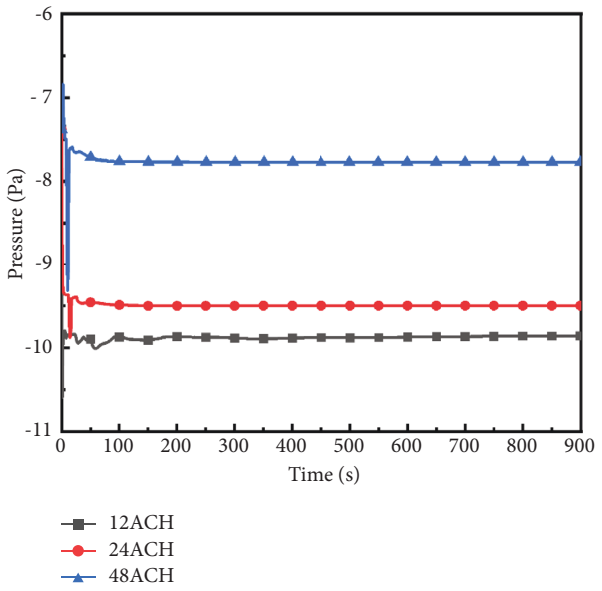

Figure 13: Pressure in 900 s in cases 12, 24, and 48 ACH.

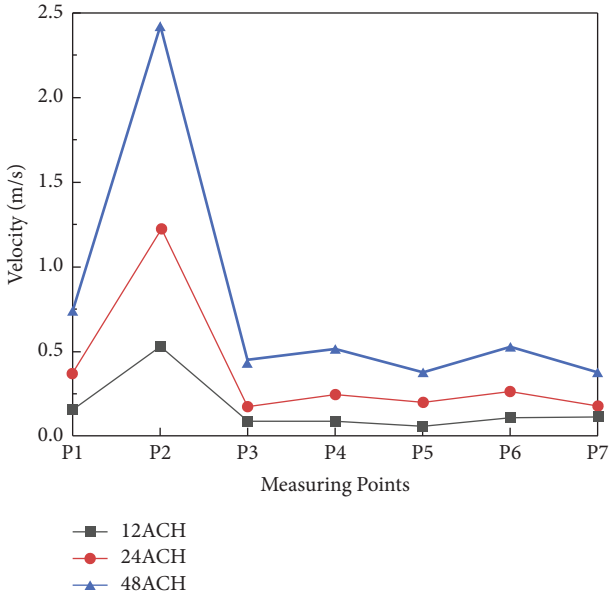

Figure 14: Velocity distribution at various locations inside the room in cases 12, 24, and 48 ACH.

In Figure 13, the pressure magnitude is constant at −10 Pa for the 12 ACH case. For the 24 ACH case, the pressure strength changes only by 0.5 Pa. When compared with the 48 ACH case, the magnitude of the visible pressure is a large change. The value ACH is the number of times that the total air volume in a room or space is completely removed and replaced in an hour. If the air in the space is either uniform or perfectly mixed, air change per hour is a measure of how many times the air within a defined space is replaced each hour. In the case of 48 ACH, the concentration of pollutants in the isolation room's air has been significantly reduced, and the larger the ACH parameter, the higher the velocity values in the isolation room leading to larger and linear with a volumetric flow rate of air.

Figure 14 illustrates the difference in velocities at various locations in the room with different cases of air change per hour. When the ACH parameters are greater, the velocity values at the measurement points are higher. Furthermore, based on visual acuity, the larger the ACH number, the greater the difference in velocity value between the highest point and the rest of the points.

The primary goal of this paper is to study the room contaminant removal performance of the HVAC system as the number of air change per hour changes. According to the numerical simulation estimates in Figure 15, the larger the ACH value, the closer the CO_2 concentration curve is to 400 ppm. The CO_2 concentration could be lowered to 581 ppm in the 12 ACH cases, 477 ppm in the 24 ACH cases, and 438 ppm in the 48 ACH cases over the 900 s. Furthermore, the rate of decrease in CO_2 concentration varies in each scenario. The system takes 300 s to stabilize the CO_2

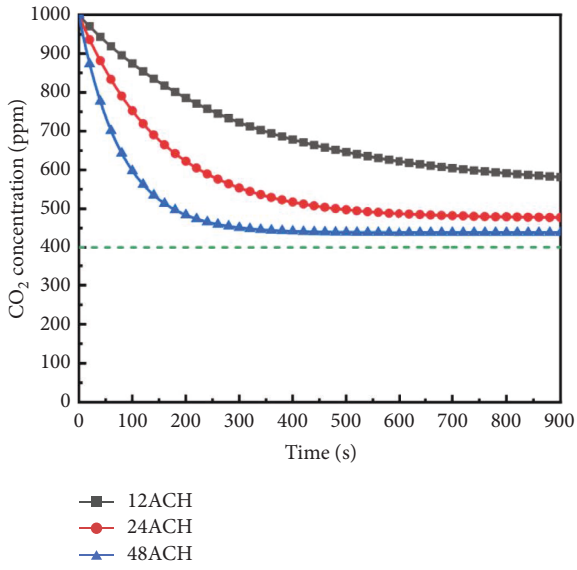

Figure 15: CO_2 concentration in cases 12, 24, and 48 ACH.

concentration value in the 48 ACH case, whereas it takes 600 s in the 24 ACH instance. As a result, the higher the number of air change per hour, the better the ability to eliminate contaminants from the room.

5. Conclusion

In this study, a portable negative pressurized isolation room with shipping containers has been carried out, and a numerical transient simulation of the main isolation room has been accomplished to understand how ventilation air is distributed and how airborne contaminants are spread throughout the room based on CO_2 concentration simulation. The aerodynamic results of airflow, as well as the CO_2 concentration, have been compared when changing air change per hour values. The numerical results revealed that the temperature in the room is suitable for people inside, and the contaminants removal performance can be improved by increasing the ACH parameter. In addition, increasing the ACH also led to an increase in the velocity of the airflow in the room. The ventilation performance of this design can be improved by changing the location of the exhaust air grilles. CFD is a useful tool for evaluating and refining designs to determine the optimum layout for ventilation system arrangement and contamination control.

Data Availability

Data are included within the article.

Conflicts of Interest

The authors declare that they have no conflicts of interest.

Acknowledgments

This research was supported by DCSELAB and funded by Vietnam National University Ho Chi Minh City (VNU-HCM) under grant number TX2022-20b-01. The authors acknowledge the support of time and facilities from Ho Chi Minh City University of Technology (HCMUT), VNU-HCM, for this study.

References

[1] M. Jayaweera, H. Perera, B. Gunawardana, and J. Manatunge, "Transmission of COVID-19 virus by droplets and aerosols: a critical review on the unresolved dichotomy," *Environmental Research*, vol. 188, Article ID 109819, 2020.

[2] Q. Wang and L. Liu, "On the critical role of human feces and public toilets in the transmission of COVID-19: evidence from China," *Sustainable Cities and Society*, vol. 75, Article ID 103350, 2021.

[3] L. Tang, M. Liu, B. Ren et al., "Transmission in home environment associated with the second wave of COVID-19 pandemic in India," *Environmental Research*, vol. 204, Article ID 111910, 2022.

[4] T. M. Habeebullah, I. H. Abd El-Rahim, and E. A. Morsy, "Impact of outdoor and indoor meteorological conditions on the COVID-19 transmission in the western region of Saudi Arabia," *Journal of Environmental Management*, vol. 288, Article ID 112392, 2021.

[5] Y.-H. Chen, J. Lei, J. Li et al., "Design characteristics on the indoor and outdoor air environments of the COVID-19 emergency hospital," *Journal of Building Engineering*, vol. 45, Article ID 103246, 2022.

[6] J. Wu and W. Weng, "COVID-19 virus released from larynx might cause a higher exposure dose in indoor environment," *Environmental Research*, vol. 199, Article ID 111361, 2021.

[7] L. Morawska, J. W. Tang, W. Bahnfleth et al., "How can airborne transmission of COVID-19 indoors be minimised?" *Environment International*, vol. 142, Article ID 105832, 2020.

[8] T.-L. Le, J.-C. Chen, B.-C. Shen, F.-S. Hwu, and H.-B. Nguyen, "Numerical investigation of the thermocapillary actuation behavior of a droplet in a microchannel," *International Journal of Heat and Mass Transfer*, vol. 83, pp. 721–730, 2015.

[9] T.-L. Le, J.-C. Chen, F.-S. Hwu, and H.-B. Nguyen, "Numerical study of the migration of a silicone plug inside a capillary tube subjected to an unsteady wall temperature gradient," *International Journal of Heat and Mass Transfer*, vol. 97, pp. 439–449, 2016.

[10] T.-L. Le, J.-C. Chen, and H.-B. Nguyen, "Numerical study of the thermocapillary droplet migration in a microchannel under a blocking effect from the heated upper wall," *Applied Thermal Engineering*, vol. 122, pp. 820–830, 2017.

[11] T.-L. Le, J.-C. Chen, and H.-B. Nguyen, "Numerical investigation of the forward and backward thermocapillary motion of a water droplet in a microchannel by two periodically activated heat sources," *Numerical Heat Transfer, Part A: Applications*, vol. 79, no. 2, pp. 146–162, 2021.

[12] T.-L. Le and N. T. Tien, "A CFD study on hydraulic and disinfection efficiencies of the body sterilization chamber," *Annals of the Romanian Society for Cell Biology*, vol. 25, no. 2, pp. 3998–4004, 2021.

[13] T. L. Le and D. T. Hong, "Computational fluid dynamics study of the hydrodynamic characteristics of a torpedo-shaped underwater glider," *Fluid*, vol. 6, no. 7, p. 252, 2021.

[14] M. Beaussier, E. Vanoli, F. Zadegan et al., "Aerodynamic analysis of hospital ventilation according to seasonal variations. A simulation approach to prevent airborne viral transmission pathway during COVID-19 pandemic," *Environment International*, vol. 158, Article ID 106872, 2022.

[15] S. Peng, Q. Chen, and E. Liu, "The role of computational fluid dynamics tools on investigation of pathogen transmission: prevention and control," *Science of the Total Environment*, vol. 746, Article ID 142090, 2020.

[16] S. Bhattacharyya, K. Dey, A. R. Paul, and R. Biswas, "A novel CFD analysis to minimize the spread of COVID-19 virus in hospital isolation room," *Chaos, Solitons & Fractals*, vol. 139, Article ID 110294, 2020.

[17] D. S. Thatiparti, U. Ghia, and K. R. Mead, "Computational fluid dynamics study on the influence of an alternate ventilation configuration on the possible flow path of infectious cough aerosols in a mock airborne infection isolation room," *Science and Technology for the Built Environment*, vol. 23, no. 2, pp. 355–366, 2016.

[18] M. F. King, C. J. Noakes, P. A. Sleigh, and M. A. Camargo-Valero, "Bioaerosol deposition in single and two-bed hospital rooms: a numerical and experimental study," *Building and Environment*, vol. 59, pp. 436–447, 2013.

[19] S. L. Miller, D. Mukherjee, J. Wilson, N. Clements, and C. Steiner, "Implementing a negative pressure isolation space within a skilled nursing facility to control SARS-CoV-2 transmission," *American Journal of Infection Control*, vol. 49, no. 4, pp. 438–446, 2021.

[20] Y. C. Shih, C. C. Chiu, and O. Wang, "Dynamic airflow simulation within an isolation room," *Building and Environment*, vol. 42, no. 9, pp. 3194–3209, 2007.

[21] P. Mahajan, A. Saco S, R. D. Kumar, and T. K. Raj R, "Airflow simulation of an isolation room using CFD technique," *International Journal of Pure and Applied Mathematics*, vol. 118, no. 18, pp. 4261–4269, 2018.

[22] S. Jacob, S. S. Yadav, and B. S. Sikawar, "Design and simulation of isolation room for a hospital," *Advances in Fluid and Thermal Engineering*, pp. 75–93, 2019.

[23] F. Wang, C. Chaerasari, D. Rakshit, I. Permana, and Kusnadar, "Performance improvement of a negative-pressurized isolation room for infection control," *Healthcare*, vol. 9, no. 8, p. 1081, 2021.

[24] J. Cho, "Investigation on the contaminant distribution with improved ventilation system in hospital isolation rooms: effect of supply and exhaust air diffuser configurations," *Applied Thermal Engineering*, vol. 148, pp. 208–218, 2019.

[25] B. Obeidat, O. F. Alrebei, I. A. Abdallah, E. F. Darwish, and A. Amhamed, "CFD analyses: the effect of pressure suction and airflow velocity on coronavirus dispersal," *Applied Sciences*, vol. 11, no. 16, p. 7450, 2021.

[26] F. Wang, I. Permana, C. Chaerasari, B. Panigrahi, and D. Rakshit, "Infection control improvement of a negative-pressurized pediatric intensive care unit," *Healthcare*, vol. 9, no. 11, p. 1500, 2021.

[27] Y. C. Tung, Y. C. Shih, and S. C. Hu, "Numerical study on the dispersion of airborne contaminants from an isolation room in the case of door opening," *Applied Thermal Engineering*, vol. 29, no. 8-9, pp. 1544–1551, 2009.

[28] G. S. N. V. K. S. N. Swamy, "Development of an indoor air purification system to improve ventilation and air quality," *Heliyon*, vol. 7, no. 10, p. e08153, Article ID e08153, 2021.

[29] M. R. Laurent and J. Frans, "Monitors to improve indoor air carbon dioxide concentrations in the hospital: a randomized crossover trial," *Science of the Total Environment*, vol. 806, Article ID 151349, 2022.

[30] W. Ha, T. F. Zabarsky, E. C. Eckstein et al., "Use of carbon dioxide measurements to assess ventilation in an acute care hospital," *American Journal of Infection Control*, vol. 50, no. 2, pp. 229–232, 2022.

[31] M. K. Kim and J. H. Choi, "Can increased outdoor CO2 concentrations impact on the ventilation and energy in buildings? A case study in Shanghai, China," *Atmospheric Environment*, vol. 210, pp. 220–230, 2019.